


Ultrasound resonance in coflowing immiscible liquids in a microchannelS. Z. Hoque¹ and A. K. Sen^{1,2,*}¹*Fluid Systems Laboratory, Department of Mechanical Engineering, Indian Institute of Technology Madras, Chennai 600036, Tamil Nadu, India*²*Micro Nano Bio-Fluidics Group, Indian Institute of Technology Madras, Chennai 600036, Tamil Nadu, India* (Received 6 June 2022; revised 23 November 2022; accepted 22 February 2023; published 6 March 2023)

We study ultrasonic resonance in a coflow system comprising a pair of immiscible liquids in a microchannel exposed to bulk acoustic waves. We show using an analytical model that there are two resonating frequencies corresponding to each of the coflowing liquids, which depend on the speed of sound and stream width of the liquid. We perform a frequency domain analysis using numerical simulations to reveal that resonance can be achieved by actuating both liquids at a single resonating frequency that depends on the speeds of sound, densities, and widths of the liquids. In a coflow system with equal speeds of sound and densities of the pair of fluids, the resonating frequency is found to be independent of the relative width of the two streams. In coflow systems with unequal speeds of sound or densities, even with matching characteristic acoustic impedances, the resonating frequency depends on the stream width ratio, and the value increases with an increase in the stream width of the liquid with a higher speed of sound. We show that a pressure nodal plane can be realized at the channel center by operating at a half-wave resonating frequency when the speeds of sound and densities are equal. However, the pressure nodal plane is found to shift away from the center of the microchannel when the speeds of sound and densities of the two liquids are unequal. The results of the model and simulations are verified experimentally via acoustic focusing of microparticles suggesting the formation of a pressure nodal plane and hence a resonance condition. Our study will find relevance in acoustofluidics involving immiscible coflow systems.

DOI: [10.1103/PhysRevE.107.035104](https://doi.org/10.1103/PhysRevE.107.035104)**I. INTRODUCTION**

The manipulation of micro-objects and liquids inside a microchannel using bulk acoustic waves (BAWs) has been widely used in applications in various fields such as chemical, medical, and biotechnology [1–15]. The physics of manipulation of micro-objects suspended in a liquid exposed to BAWs is well studied [16–20]. In this context, the formation of acoustic resonance modes that offer a large actuation force is advantageous for handling such objects in microfluidics [21]. Typically, for a single liquid, the microchannel width is maintained equal to the half-wavelength of the acoustic wave; therefore, the pressure nodal plane (NP) is formed at the center of the microchannel. Depending on the acoustic contrast between the particle and the suspending medium, the particle will move toward the pressure node at the channel center or the pressure antinode at the walls. The particle experiences maximum acoustic radiation force at the resonance modes as the acoustic power delivered from a transducer to the device is highest. The locations of pressure nodes and the half-wave resonance mode are well understood for density interfaces [13,14,22–24]. In inhomogeneous and miscible liquids, the density, compressibility, and fluid viscosity vary spatially as a function of solute concentration. It was shown experimentally that the speed of sound in the media does not depend on the solute concentration, and therefore, the half-wave resonance

mode can be readily achieved in the case of miscible inhomogeneous liquids [25]. The effect of acoustic force density and streaming velocity field suppression in a miscible inhomogeneous liquid system exposed to BAWs has been reported [26,27].

In immiscible fluid systems [28–34], there is a discontinuity in the density and speed of sound of the liquids resulting in the reflection and transmission of the acoustic waves at the fluid interface [5]. A sudden jump in the acoustic properties can significantly alter the total acoustic field, and therefore, obtaining the half-wave resonance conditions in immiscible coflow systems is extremely challenging. In contrast to a single-phase system or a miscible inhomogeneous system in which a pressure NP can be obtained theoretically via velocity boundary conditions at the walls [21], the reflection and transmission of the waves at the interface must be considered in the case of an immiscible coflow system. Recently we reported the relocation of liquid streams in an immiscible coflow system exposed to BAWs inside a microchannel [35] and explained the observed phenomenon in terms of the impedance contrast between the liquids. On-demand stream-drop transition and coalescence of aqueous droplets in an immiscible coflow system exposed to BAWs were also studied [5,36]. However, acoustic resonance modes in immiscible coflow systems exposed to BAWs have not been explored to date, which is the focus of the present work. Further, the formation of the pressure NP which is central to acoustophoretic migration and focusing in acoustofluidics systems is also not well understood, which is investigated here. We study ultrasonic

*Corresponding author: ashis@iitm.ac.in

resonance modes in a coflow system comprising a pair of immiscible liquids in a microchannel exposed to bulk acoustic waves using theoretical modeling, numerical simulations, and experiments.

II. THEORETICAL

In this section, we first discuss the derivation of the Helmholtz equation for a steady acoustic field applied to a compressible Newtonian liquid. The Helmholtz equation is obtained using the first-order perturbation theory from the fundamental equations of fluid mechanics and thermodynamics relations expressing pressure in terms of density as follows [18]:

$$p = p(\rho), \quad (1a)$$

$$\frac{\partial \rho_f}{\partial t} = -\nabla \cdot (\rho_f \mathbf{u}_f), \quad (1b)$$

$$\rho_f \frac{\partial \mathbf{u}_f}{\partial t} + \rho_f (\mathbf{u}_f \cdot \nabla) \mathbf{u}_f = -\nabla p + \mu \nabla^2 \mathbf{u}_f + \beta \mu \nabla (\nabla \cdot \mathbf{u}_f) + \mathbf{F}_b, \quad (1c)$$

where ρ_f and \mathbf{u}_f are, respectively, the density and liquid velocity, p is the liquid pressure, μ is shear viscosity, β is the ratio of the bulk viscosity to the dynamic viscosity of the fluid and \mathbf{F}_b is the body force acting on the liquid. We have neglected external force fields such as gravity and electromagnetism in the present study.

Let the acoustic wave create tiny perturbations to the fluid velocity, pressure, and density. The perturbed values are negligible compared to the corresponding values at thermal equilibrium, so the first-order perturbation theory can be applied to derive the acoustic wave equation. We also assume the process to be adiabatic and neglect the role of heat transfer in acoustic wave propagation. Therefore, the thermodynamics state can be described by pressure as considered in Eq. (1). Before applying the perturbation due to acoustic wave, let us consider a steady fluid, i.e., initially, the liquid is at rest, with constant density ρ_0 and pressure p_0 . We consider that acoustic perturbation is used to actuate the fluid, and the microchannel walls are considered to be rigid [37]. By including the perturbation terms up to the first order (subscript 1), the various fields are obtained as follows [21]:

$$p = p_0 + p_1 + \dots, \quad (2a)$$

$$\rho_f = \rho_0 + \rho_1 + \dots, \quad (2b)$$

$$\mathbf{u}_f = \mathbf{0} + \mathbf{v}_1 + \dots, \quad (2c)$$

where the subscripts 0 and 1 represent the quiescent (steady) and first-order perturbed states, respectively. Since we are interested in understanding the acoustic pressure field for coflowing liquids inside a microchannel, we have neglected the higher-order terms in Eqs. (2). The second-order terms are important to explain the acoustic streaming effects which are of slow timescale phenomena compared to the fast timescale involved in the oscillation of the acoustic wave [21]. Since we have assumed sound waves to be adiabatic, the first-order pressure field can be written in terms of density perturbation by performing the isentropic expansion of pressure about the

steady state,

$$p = p_0 + \left(\frac{\partial p}{\partial \rho} \right)_0 (\rho - \rho_0) + \dots = p_0 + c_0^2 \rho_1 + \dots, \quad (3)$$

where c_0 is the isentropic speed of sound in the fluid. By truncating the above expression up to the first order, we can express the first-order pressure field as

$$p_1 = c_0^2 \rho_1. \quad (4)$$

Now simplifying the continuity equation [i.e., Eq. 1(b)] using the first-order perturbations [Eqs. (2)] as follows:

$$\frac{\partial (\rho_0 + \rho_1)}{\partial t} = -\nabla \cdot [(\rho_0 + \rho_1)(\mathbf{v}_1)] \quad (5a)$$

$$= -\rho_0 \nabla \cdot \mathbf{v}_1 - \nabla \cdot (\rho_1 \mathbf{v}_1) \quad (5b)$$

and neglecting the second-order terms (product of the first-order terms), we obtained the first-order continuity equation,

$$\frac{\partial \rho_1}{\partial t} = -\rho_0 \nabla \cdot \mathbf{v}_1 \quad (5c)$$

Similarly, the momentum equation (1(c)) is perturbed using the first-order perturbations,

$$\begin{aligned} (\rho_0 + \rho_1) \frac{\partial \mathbf{v}_1}{\partial t} + (\rho_0 + \rho_1)(\mathbf{v}_1 \cdot \nabla) \mathbf{v}_1 \\ = -\nabla(p_0 + p_1) + \mu \nabla^2 \mathbf{v}_1 + \beta \mu \nabla (\nabla \cdot \mathbf{v}_1), \end{aligned} \quad (6a)$$

or

$$\begin{aligned} \rho_0 \frac{\partial \mathbf{v}_1}{\partial t} + \rho_1 \frac{\partial \mathbf{v}_1}{\partial t} + \rho_0 (\mathbf{v}_1 \cdot \nabla) \mathbf{v}_1 + \rho_1 (\mathbf{v}_1 \cdot \nabla) \mathbf{v}_1 \\ = -\nabla p_1 + \mu \nabla^2 \mathbf{v}_1 + \beta \mu \nabla (\nabla \cdot \mathbf{v}_1), \end{aligned} \quad (6b)$$

Neglecting the second-order terms and using Eq. (4), we get

$$\rho_0 \frac{\partial \mathbf{v}_1}{\partial t} = -c_0^2 \nabla \rho_1 + \mu \nabla^2 \mathbf{v}_1 + \beta \mu \nabla (\nabla \cdot \mathbf{v}_1). \quad (6c)$$

Now by taking the derivative of Eq. 5(c) with time and using Eq. 6(c), we have

$$\frac{\partial^2 \rho_1}{\partial t^2} = -\nabla \cdot \left(\rho_0 \frac{\partial \mathbf{v}_1}{\partial t} \right) \quad (7a)$$

$$= -\nabla \cdot [-c_0^2 \nabla \rho_1 + \mu \nabla^2 \mathbf{v}_1 + \beta \mu \nabla (\nabla \cdot \mathbf{v}_1)] \quad (7b)$$

$$= c_0^2 \nabla^2 \rho_1 - \mu \nabla^2 (\nabla \cdot \mathbf{v}_1) - \beta \mu \nabla^2 (\nabla \cdot \mathbf{v}_1) \quad (7c)$$

$$= c_0^2 \nabla^2 \rho_1 - \mu (1 + \beta) \nabla^2 (\nabla \cdot \mathbf{v}_1) \quad (7d)$$

$$= c_0^2 \nabla^2 \rho_1 + \mu (1 + \beta) / \rho_0 \nabla^2 \left(\frac{\partial \rho_1}{\partial t} \right) \quad (7e)$$

$$= c_0^2 \left(1 + \frac{\mu (1 + \beta)}{\rho_0 c_0^2} \frac{\partial}{\partial t} \right) \nabla^2 \rho_1. \quad (7f)$$

To ease mathematical treatment, let us assume the harmonic time dependence of all fields,

$$\rho_1(\mathbf{r}, t) = \tilde{\rho}_1(\mathbf{r}) e^{-i\omega t}, \quad (8a)$$

$$p_1(\mathbf{r}, t) = \tilde{p}_1(\mathbf{r}) e^{-i\omega t}, \quad (8b)$$

$$v_1(\mathbf{r}, t) = \tilde{v}_1(\mathbf{r}) e^{-i\omega t}, \quad (8c)$$

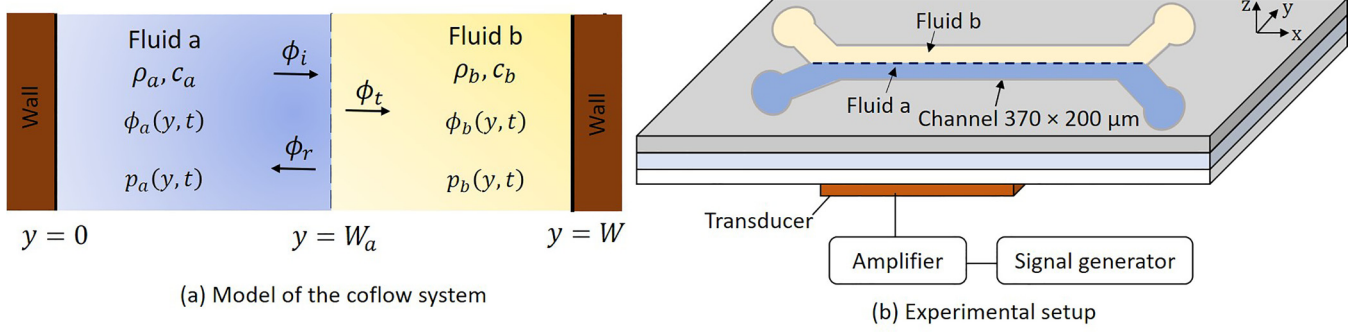


FIG. 1. (a) Schematic of the layered two-liquid system exposed to BAWs considered in the theoretical model. (b) Schematic of the experimental setup used for studying ultrasound resonance in an immiscible coflow system.

where $\omega = 2\pi f$ is the angular frequency, and f is the actuation frequency of the acoustic wave. Using the harmonic fields and Eq. (4), we further simplify Eq. (7f) as follows [21]:

$$\frac{\partial^2(\tilde{\rho}_1 e^{-i\omega t})}{\partial t^2} = c_0^2 \left(1 + \frac{\mu(1+\beta)}{\rho_0 c_0^2} \frac{\partial}{\partial t} \right) \nabla^2(\tilde{\rho}_1 e^{-i\omega t}), \quad (9a)$$

or

$$-\omega^2 \tilde{\rho}_1 e^{-i\omega t} = c_0^2 \left(1 + \frac{\mu(1+\beta)}{\rho_0 c_0^2} \times (-i\omega) e^{-i\omega t} \right) \nabla^2 \tilde{\rho}_1, \quad (9b)$$

or

$$-\omega^2 \tilde{\rho}_1 e^{-i\omega t} = c_0^2 \left(1 + \frac{\mu(1+\beta)}{\rho_0 c_0^2} \times (-i\omega) e^{-i\omega t} \right) \nabla^2 \tilde{\rho}_1, \quad (9c)$$

or

$$-\frac{\omega^2}{c_0^2} p_1 = \left(1 + \frac{\mu(1+\beta)}{\rho_0 c_0^2} \times (-i\omega) \right) \nabla^2 (c_0^2 \tilde{\rho}_1 e^{-i\omega t}) \quad (9d)$$

or

$$-k_0^2 p_1 = \left(1 - i \frac{\mu(1+\beta)\omega}{\rho_0 c_0^2} \right) \nabla^2 p_1, \quad (9e)$$

or

$$-k_0^2 p_1 = (1 - i2\gamma) \nabla^2 p_1, \quad (9f)$$

where k_0 is the real-valued wave number and γ is the damping factor of the acoustic wave defined as $\gamma = (1+\beta)\mu\omega/(2\rho_0 c_0^2)$. For the inviscid case, ($\gamma \ll 1$), the Helmholtz equation can be written as

$$\nabla^2 p_1 = -k_0^2 p_1. \quad (10)$$

The 1D Helmholtz equation is given as

$$\frac{\partial^2 p_1}{\partial y^2} = -k_0^2 p_1. \quad (11)$$

Considering 1D BAWs, the fundamental properties of the acoustic resonance modes in the case of a single liquid are extensively studied by Bruus [21]. The planar resonator can be modeled in an approximate 1D device where the different components are composed of different layers that are driven by a transducer, modeled using a simple forcing function at the boundary between the layers [38]. Here the acoustic resonance modes of a layered two-liquid system are studied

using the former approach. Let us consider two planar walls perpendicular to the xz plane at $y = 0$ and $y = W$ and a pair of immiscible liquids, i.e., liquid a and liquid b , present between the walls in a parallel configuration [see Fig. 1(a)]. Fluid a is located between $y = 0$ and $y = W_a$, with the interface between the liquids is located at $y = W_a$. The acoustic waves are propagating along the y direction, and so the interface is perpendicular to the acoustic wave direction. We seek a solution of the 1D Helmholtz equation [Eq. (11)] for inviscid fluid, as $\mathbf{v}_1 = f(y)e^{-i\omega t} \mathbf{e}_y$ and, $\nabla \times \mathbf{v}_1 = 0$, so that $\mathbf{v}_1 = \nabla \phi_1$, where ϕ_1 is the first-order velocity potential. Here for inviscid flow, the relationship between the first-order velocity potential and pressure is given by $\phi_1 = -\frac{i}{(\rho_0 \omega)} p_1$, where ρ_0 is the zeroth-order density of fluid.

The small oscillations of the planar walls in the y direction are modeled using the velocity boundary conditions,

$$v_a(0, t) = -\omega l e^{-i\omega t}, \quad v_b(W, t) = +\omega l e^{-i\omega t}, \quad (12)$$

where v_a and v_b are the velocity of oscillations of the walls adjacent to the liquid a and liquid b due to acoustic actuation, respectively, l is the displacement amplitude of oscillation, which is considered to be very small compared to the width of the channel (~ 0.1 nm), and thereby, we can neglect the movement of the walls, ω is the frequency of oscillation, and t is time. The density and speed of sound in fluid a are ρ_a , c_a and in fluid b are ρ_b , c_b respectively. Consider a sound wave traveling through liquid a and at normal incidence to the interface, represented by

$$\phi_i = A_a e^{+ik_a y} e^{-i\omega t}, \quad (13)$$

where $k_a = \omega/c_a$ and A_a is the amplitude of the incident wave. The sound wave is generally partially reflected and partly transmitted at the liquid-liquid interface. Let the reflected wave be

$$\phi_r = B_a e^{-ik_a y} e^{-i\omega t} \quad (14)$$

and the transmitted wave be

$$\phi_t = A_b e^{+ik_b y} e^{-i\omega t}, \quad (15)$$

where k_b is the wave number corresponding to liquid b . B_a and A_b are the coefficients of the reflected and the transmitted wave, respectively. The boundary conditions for the first-order acoustic fields at the interface are that the velocities and normal stresses are continuous across the interface,

$v_a(W_a, t) = v_b(W_a, t)$ and $p_a(W_a, t) = p_b(W_a, t)$. We can reformulate the boundary conditions in terms of velocity potential as

$$\partial_y \phi_a(W_a, t) = \partial_y \phi_b(W_a, t) \text{ and } \rho_a \phi_a(W_a, t) = \rho_b \phi_b(W_a, t). \tag{16}$$

Further, the transmitted wave is reflected from the other wall at $y = W$. The first-order velocity potential ϕ_1 for the acoustic field takes the form

$$\phi_1(y, t) = \begin{cases} \phi_a(y, t) = (A_a e^{ik_a y} + B_a e^{-ik_a y}) e^{-i\omega t}, & 0 < y < W_a \\ \phi_b(y, t) = (A_b e^{ik_b y} + B_b e^{-ik_b y}) e^{-i\omega t}, & W_a < y < W \end{cases} \tag{17}$$

The unknown coefficients A_a , B_a , A_b , and B_b are determined using the four boundary conditions given by Eqs. (12) and (16) as

$$A_a = -\frac{i\omega l [k_a \rho_b (e^{i2k_b W_a} + e^{i2k_b W} + 2e^{ik_a W_a} e^{ik_b W_a} e^{ik_b W}) + k_b \rho_a (e^{i2k_b W_a} - e^{i2k_b W})]}{k_a [k_a \rho_b (e^{i2k_b W_a} + e^{i2k_b W})(1 - e^{i2k_a W_a}) + k_b \rho_a (e^{i2k_b W_a} - e^{i2k_b W})(1 + e^{i2k_a W_a})]}, \tag{18a}$$

$$B_a = -\frac{i\omega l e^{ik_a W_a} [k_a \rho_b (e^{i2k_b W_a} + e^{i2k_b W} + 2e^{ik_a W_a} e^{i2k_b W} + 2e^{ik_b W_a} e^{ik_b W}) + k_b \rho_a (e^{i2k_b W_a} - e^{i2k_b W})]}{k_a [k_a \rho_b (e^{i2k_b W_a} + e^{i2k_b W})(1 - e^{i2k_a W_a}) + k_b \rho_a (e^{i2k_b W_a} - e^{i2k_b W})(1 + e^{i2k_a W_a})]}, \tag{18b}$$

$$A_b = -\frac{i\omega l [k_a \rho_b (-e^{ik_b W} + e^{i2k_a W_a} e^{ik_b W}) + k_b \rho_a (e^{ik_b W} + 2e^{ik_a W_a} e^{ik_b W_a} + e^{i2k_a W_a} e^{ik_b W})]}{k_b [k_a \rho_b (e^{i2k_b W_a} + e^{i2k_b W})(1 - e^{i2k_a W_a}) + k_b \rho_a (e^{i2k_b W_a} - e^{i2k_b W})(1 + e^{i2k_a W_a})]}, \tag{18c}$$

$$B_b = -\frac{i\omega l e^{ik_b W_a} e^{ik_b W} [k_a \rho_b (e^{i2k_b W_a} - e^{i2k_a W_a} e^{ik_b W_a}) + k_b \rho_a (e^{i2k_b W_a} + 2e^{ik_a W_a} e^{ik_b W} + e^{i2k_a W_a} e^{ik_b W_a})]}{k_b [k_a \rho_b (e^{i2k_b W_a} + e^{i2k_b W})(1 - e^{i2k_a W_a}) + k_b \rho_a (e^{i2k_b W_a} - e^{i2k_b W})(1 + e^{i2k_a W_a})]}. \tag{18d}$$

Now we can obtain the velocity fields in the liquids a and b as

$$v_a(y, t) = \frac{\partial \phi_a}{\partial y} = ik_a (A_a e^{ik_a y} - B_a e^{-ik_a y}) e^{-i\omega t}, \tag{19a}$$

$$v_b(y, t) = \frac{\partial \phi_b}{\partial y} = ik_b (A_b e^{ik_b y} - B_b e^{-ik_b y}) e^{-i\omega t}. \tag{19b}$$

Using the coefficients defined in Eqs. (18), the velocity fields can be expressed as

$$v_a(y, t) = \left\{ \frac{\omega l [k_a \rho_b (e^{i2k_b W_a} + e^{i2k_b W} + 2e^{ik_a W_a} e^{ik_b W_a} e^{ik_b W}) + k_b \rho_a (e^{i2k_b W_a} - e^{i2k_b W})]}{[k_a \rho_b (e^{i2k_b W_a} + e^{i2k_b W})(1 - e^{i2k_a W_a}) + k_b \rho_a (e^{i2k_b W_a} - e^{i2k_b W})(1 + e^{i2k_a W_a})]} e^{ik_a y} - \frac{\omega l e^{ik_a W_a} [k_a \rho_b (e^{i2k_b W_a} + e^{i2k_b W} + 2e^{ik_a W_a} e^{i2k_b W} + 2e^{ik_b W_a} e^{ik_b W}) + k_b \rho_a (e^{i2k_b W_a} - e^{i2k_b W})]}{[k_a \rho_b (e^{i2k_b W_a} + e^{i2k_b W})(1 - e^{i2k_a W_a}) + k_b \rho_a (e^{i2k_b W_a} - e^{i2k_b W})(1 + e^{i2k_a W_a})]} e^{-ik_a y} \right\} e^{-i\omega t}, \tag{20a}$$

$$v_b(y, t) = \left\{ \frac{\omega l [k_a \rho_b (-e^{ik_b W} + e^{i2k_a W_a} e^{ik_b W}) + k_b \rho_a (e^{ik_b W} + 2e^{ik_a W_a} e^{ik_b W_a} + e^{i2k_a W_a} e^{ik_b W})]}{[k_a \rho_b (e^{i2k_b W_a} + e^{i2k_b W})(1 - e^{i2k_a W_a}) + k_b \rho_a (e^{i2k_b W_a} - e^{i2k_b W})(1 + e^{i2k_a W_a})]} e^{ik_b y} - \frac{\omega l e^{ik_b W_a} e^{ik_b W} [k_a \rho_b (e^{i2k_b W_a} - e^{i2k_a W_a} e^{ik_b W_a}) + k_b \rho_a (e^{i2k_b W_a} + 2e^{ik_a W_a} e^{ik_b W} + e^{i2k_a W_a} e^{ik_b W_a})]}{[k_a \rho_b (e^{i2k_b W_a} + e^{i2k_b W})(1 - e^{i2k_a W_a}) + k_b \rho_a (e^{i2k_b W_a} - e^{i2k_b W})(1 + e^{i2k_a W_a})]} e^{-ik_b y} \right\} e^{-i\omega t}, \tag{20b}$$

The first-order acoustic pressure field can be defined in terms of velocity potential as $p_a = i\omega \rho_b \phi_a$ and $p_b = i\omega \rho_b \phi_b$. Using this, we can write the first-order acoustic pressure field for liquid a and liquid b as

$$p_a(y, t) = \left\{ \frac{\omega^2 \rho_a l [k_a \rho_b (e^{i2k_b W_a} + e^{i2k_b W} + 2e^{ik_a W_a} e^{ik_b W_a} e^{ik_b W}) + k_b \rho_a (e^{i2k_b W_a} - e^{i2k_b W})]}{k_a [k_a \rho_b (e^{i2k_b W_a} + e^{i2k_b W})(1 - e^{i2k_a W_a}) + k_b \rho_a (e^{i2k_b W_a} - e^{i2k_b W})(1 + e^{i2k_a W_a})]} e^{ik_a y} - \frac{\omega^2 \rho_a l e^{ik_a W_a} [k_a \rho_b (e^{i2k_b W_a} + e^{i2k_b W} + 2e^{ik_a W_a} e^{i2k_b W} + 2e^{ik_b W_a} e^{ik_b W}) + k_b \rho_a (e^{i2k_b W_a} - e^{i2k_b W})]}{k_a [k_a \rho_b (e^{i2k_b W_a} + e^{i2k_b W})(1 - e^{i2k_a W_a}) + k_b \rho_a (e^{i2k_b W_a} - e^{i2k_b W})(1 + e^{i2k_a W_a})]} e^{-ik_a y} \right\} e^{-i\omega t}, \tag{21a}$$

$$p_b(y, t) = \left\{ \frac{\omega^2 \rho_b l [k_a \rho_b (-e^{ik_b W} + e^{i2k_a W_a} e^{ik_b W}) + k_b \rho_a (e^{ik_b W} + 2e^{ik_a W_a} e^{ik_b W_a} + e^{i2k_a W_a} e^{ik_b W})]}{k_b [k_a \rho_b (e^{i2k_b W_a} + e^{i2k_b W})(1 - e^{i2k_a W_a}) + k_b \rho_a (e^{i2k_b W_a} - e^{i2k_b W})(1 + e^{i2k_a W_a})]} e^{ik_b y} - \frac{\omega^2 \rho_b l e^{ik_b W_a} [k_a \rho_b (e^{i2k_b W_a} - e^{i2k_a W_a} e^{ik_b W_a}) + k_b \rho_a (e^{i2k_b W_a} + 2e^{ik_a W_a} e^{ik_b W} + e^{i2k_a W_a} e^{ik_b W_a})]}{k_b [k_a \rho_b (e^{i2k_b W_a} + e^{i2k_b W})(1 - e^{i2k_a W_a}) + k_b \rho_a (e^{i2k_b W_a} - e^{i2k_b W})(1 + e^{i2k_a W_a})]} e^{-ik_b y} \right\} e^{-i\omega t}. \tag{21b}$$

The acoustic velocity field acquires significantly high amplitudes in the acoustic resonance modes and thus contains a large amount of the stored energy. For a single liquid case, the resonance modes can be theoretically determined by minimizing the denominator of the velocity term. In analogous to the single-fluid case, we obtained the resonance condition by minimizing the

denominator of Eqs. (20) as $e^{ik_a W_a} = \pm e^{-ik_a W_a}$ or $\sin(k_a W_a) = 0$, which gives $k_a W_a = m\pi$, $m = 1, 2, 3, \dots$, and $e^{ik_b(W-W_a)} = \pm e^{-ik_b(W-W_a)}$ or $\sin[k_b(W-W_a)] = 0$, which gives $k_b(W-W_a) = n\pi$, $n = 1, 2, 3, \dots$,

$$k_a = \frac{m\pi}{W_a}, \quad (22a)$$

$$k_b = \frac{n\pi}{(W-W_a)}. \quad (22b)$$

The corresponding resonating frequencies for the liquid a and liquid b are given as

$$\omega_{a_m} = c_a k_{a_m} = c_a \frac{m\pi}{W_a}, \quad (23a)$$

$$\omega_{b_n} = c_b k_{b_n} = c_b \frac{n\pi}{(W-W_a)}. \quad (23b)$$

The acoustic resonance occurs at the wave numbers, $k_{a_m} = \frac{m\pi}{W_a}$, $m \in \mathbb{N}$ and $k_{b_n} = \frac{n\pi}{(W-W_a)}$, $n \in \mathbb{N}$, where \mathbb{N} is a natural number. For $m = 1 = n$, we obtained a half-wave resonance condition inside the microchannel. The half-wave resonance mode is the condition where the acoustic pressure node is formed at the channel center, and the pressure antinodes are located at the channel walls. Thus theoretically we have two actuation frequencies for the two different liquids, $f_a = c_a/(2W_a)$ and $f_b = c_b/[2(W-W_a)]$, to establish resonance in the case of a layered two-liquid system exposed to 1D BAWs. Suppose a coflow system can be simultaneously actuated at the two different frequencies, each corresponding to the individual liquid; in that case, a half-wave pressure NP with equal pressure amplitudes in both liquids can be achieved. It is interesting to note that the resonating frequencies are a function of the relative widths of the liquids. Since the acoustic parameters are different for each fluid, the resonant frequency for each fluid, obtained using the theoretical model, will be different. Theoretically, in a two-fluid system, a half-wave resonance condition can be achieved when each fluid is simultaneously actuated with the corresponding resonating frequency. However, this is not practically feasible. Therefore, we performed numerical simulations to find a single half-wave resonating frequency for the two-fluid system. Further, if the density and speed of sound in the two liquids are equal, then the interface location becomes irrelevant, and, in that case, the problem becomes trivial as it is the same as the 1D inviscid liquid case. For liquids with $c_a = c_b = c_0$ and, $\rho_a = \rho_b = \rho_f$, the above analysis gives rise to a single frequency, i.e., $k = k_a$ and the half-wave resonance condition becomes, $k = \frac{m\pi}{W}$ or $f = \frac{c_0}{2W}$. In the present work, we have neglected the losses, viz., loss due to viscous dissipation, viscous friction in the acoustic boundary layer, and the radiative loss of the acoustic wave into the chip holder, surrounding air, and inlet and outlet tubes [21]. Therefore, pressure amplitudes from the theoretical model will be overpredicted as compared to that from full-chip numerical simulations that consider the losses and the experimental device.

III. NUMERICAL

The acoustic eigenmodes are analyzed for a 3D microchannel filled with coflowing liquids to gain insight into acoustic resonances. The ultrasonic resonance modes are obtained by solving a 3D numerical model which is described below. The

Helmholtz equation given by Eq. (10) is solved to determine the acoustic pressure eigenmodes, $p_1 = \tilde{p}_1(r)e^{-i\omega t}$, by considering appropriate boundary conditions. In the case of an immiscible coflow system, a part of the plane wave traveling through fluid a will get reflected from the fluid-fluid interface, and the other part will be transmitted to fluid b . The first-order velocity field and normal stresses are considered to be continuous at the fluid-fluid interface. The boundary conditions [given by Eq. (16)] are used to obtain the background 1D pressure field as a sum of the incident and reflected waves [39],

$$p^b = p_{in}[R\cos(ky + \omega t) + \cos(\omega t - ky)], \quad (24a)$$

where R is the reflection coefficient defined as $R = (Z_a - Z_b)/(Z_a + Z_b)$, Z_a , and Z_b are, respectively, the characteristic acoustic impedance in liquid a and liquid b . Here p_{in} is the amplitude of the incoming background pressure wave. In acoustophoresis, a resonating frequency of MHz range is applied to obtain half-wave resonance in a microchannel of submillimeter width, and the amplitude of the acoustic pressure field is of the order, $p_{in} \sim 1$ MPa [37]. The corresponding velocity field is given by [39]

$$v^b = \frac{k p_{in}}{\rho \omega} [\cos(\omega t - ky) - R\cos(ky + \omega t)]. \quad (24b)$$

Typically there is a timescale required for the build-up of an unsteady acoustic resonance field, and for BAW devices the build-up time scales as $\tau_E = Q/\omega$ [37], where Q is the quality factor of the acoustic wave. Since it is difficult to predict the Q factor for a two-fluids case, for our experimental system we assume the value to be ≈ 1000 [21], and we obtained the buildup resonance timescale as $\tau_E \approx 80$ μ s where the resonating frequency of the transducer is 2 MHz. The flow rate of the coflowing fluids scales as $Q \approx 10$ μ l/min. Therefore, we can define the average strain rate as $\bar{\gamma} = Q/W^2 H$, where W is the width and H is the height of the microchannel [40]. The characteristic timescale for the coflowing fluids scales as $t_f = \frac{W^2 H}{Q} \sim 0.25$ s. Since the timescale for acoustic build-up resonance is in microseconds, which is much smaller than the characteristic flow timescale, which is in hundreds of milliseconds, in the present case the acoustic fields can be considered to be steady. It was shown that, as build-up time increases (≥ 290 μ s), the unsteady time-averaged acoustic field converges to the well-known steady time-averaged solution calculated in the frequency domain [37]. In the present case, our

TABLE I. Properties of liquids used in experiments.

Material	Density (kg/m ³)		Speed of sound, c (m/s)			Impedance, Z [kg/(m ² s)]			
Silicon wafer	8490		2330			19781700			
Borosilicate glass	5560		2230			12398800			
Liquid a	Liquid b	ρ_a (kg/m ³)	ρ_b (kg/m ³)	ρ_a/ρ_b	c_a (m/s)	c_b (m/s)	c_a/c_b	Z_a	Z_b
Mineral oil	Silicone oil	858	991	0.8566	1440	1032	1.395	1235520	1022712
Olive oil	Silicone oil	915	991	0.923	1430	1032	1.386	1308450	1022712
Dextran (10% wt.)	PEG (5% wt.)	1050	1005	1.045	1581	1540	1.027	1660050	1547700
Mineral oil	Olive oil	858	915	0.937	1440	1430	1.007	1317600	1226940

focus is to predict half-wave resonating frequency for a two-fluid system using eigenfrequency analysis in the frequency domain. The total acoustic pressure field for a two-fluid system is obtained in the frequency domain for a given background pressure field using 3D simulations. The microchannel wall boundary conditions have a significant effect on the resonance modes. Typically, there are three different ways of defining the wall boundary conditions: soft wall, hard wall, or lossy wall [35]. In the present case, we see that the silicon and borosilicate substrate impedances are one order of magnitude higher than the impedances of the individual liquids used (see Table I). Therefore, in the present simulations, it is appropriate to use the hard wall boundary condition, which is given as

$$\mathbf{n} \cdot \nabla p_1 = 0, \quad (25)$$

where \mathbf{n} is the unit normal vector at the interface. Equation (10) is solved in COMSOL Multiphysics to obtain the acoustic eigenmodes using the background pressure and velocity fields given by Eqs. (24).

IV. EXPERIMENTAL

We have used a through-etched glass-silicone device comprising a straight microchannel, two inlets, and two outlets [see Fig. 1(b)]. The straight channel has a length of 20 mm and a cross section of 370 $\mu\text{m} \times 200 \mu\text{m}$. The details of the fabrication of the device are described elsewhere [18,19]. The device is actuated by driving a piezoelectric transducer with an AC voltage by sweeping actuation frequency from 1.300 to 2.900 MHz. Pulsation-free pumps (neMESYS Cetoni GmbH pumps) are used to infuse the liquids inside the microchannel at different flow rates depending upon the pair of liquids used so that a stable coflow interface is established. The properties of the liquids used in our experiments are presented in Table I. Polystyrene particles of radius 20 μm are used to observe the acoustic focusing of particles when resonance is achieved and a pressure NP is formed.

V. RESULTS AND DISCUSSION

Three-dimensional numerical simulations are performed to understand the nature of acoustic resonance conditions in a coflow system inside a rectangular channel of width $w = 375 \mu\text{m}$, height $h = 200 \mu\text{m}$, and length $l = 2 \text{ mm}$. As described in Sec. III, we solve the Helmholtz equation in the frequency domain by considering hard wall boundary conditions [21] to predict the acoustic eigenmodes of the coflowing

liquids. The background pressure field given by Eqs. (24) is used to actuate the whole system, and the amplitude of the background pressure is taken to be $p_{\text{in}} = 5.965 \text{ MPa}$. The total acoustic field is obtained via an eigenfrequency analysis for different coflow systems, which is presented in Fig. 2. We find that for a polyethylene glycol (PEG)-dextran system with a width ratio $W_a/W = 0.35$, the pressure node is located at the center of the microchannel at an actuation frequency of $f = 2.070 \text{ MHz}$ [see Fig. 2(a)]. Similarly, for the same width ratio, the pressure node is obtained for the mineral oil-olive oil system at an actuation frequency of $f = 1.890 \text{ MHz}$ [see Fig. 2(b)]. The pressure field contours at different frequencies obtained from simulations for mineral oil-silicone oil with $W_a/W = 0.35$ are presented in Appendix A. The 1D pressure field along the axial direction is plotted as a function of channel width for different frequencies. We observe that a half-wave pressure node is formed for an actuation frequency of 1.573 MHz, which is taken as the resonating frequency of the two-fluid system. At actuation frequencies of 1.5 and 1.6 MHz, we do not observe the half-wave resonance condition, and the pressure amplitudes drop significantly compared to the resonating case (see Appendix A). The variation of maximum pressure amplitude (P_{max}) as a function of actuation frequency for different stream width ratios is presented in Fig. 2. It is found that when the speeds of sound and densities of the liquids are comparable, $(c_a/c_b) = 1$ and $(\rho_a/\rho_b) = 1$, the resonating frequencies at which the maximum pressure amplitude (i.e., half wave resonance) is obtained, converge to a single value and are independent of the stream width ratios. The resonating frequency for PEG-dextran and mineral oil-olive oil is obtained as 2.07 and 1.90 MHz, respectively.

When the speeds of sound or densities differ significantly, i.e., mineral oil-silicone oil and olive oil-silicone oil combinations, the half-wave resonance mode can occur over a range of frequencies, depending on the stream width ratio [see Figs. 2(c) and 2(d)]. It is to be noted that for a given coflow system, irrespective of the stream width ratio, the resonating frequency falls between the resonating frequencies corresponding to the two individual liquids. The resonating frequency for mineral oil-silicone oil coflow system falls in the range $f_{mi} = 1.920 \text{ MHz}$ and $f_{si} = 1.375 \text{ MHz}$. Similarly, the resonating frequency for the silicone oil-olive oil combination lies in the range $f_{si} = 1.375 \text{ MHz}$ and $f_{ol} = 1.970 \text{ MHz}$. Further, we show that the resonating frequency varies with the stream width ratio for liquids having $(c_a/c_b) \neq 1$ or $(\rho_a/\rho_b) \neq 1$ even if there is a match in the characteristic impedances of the liquids, i.e., $Z_a = Z_b$; see Appendix B.

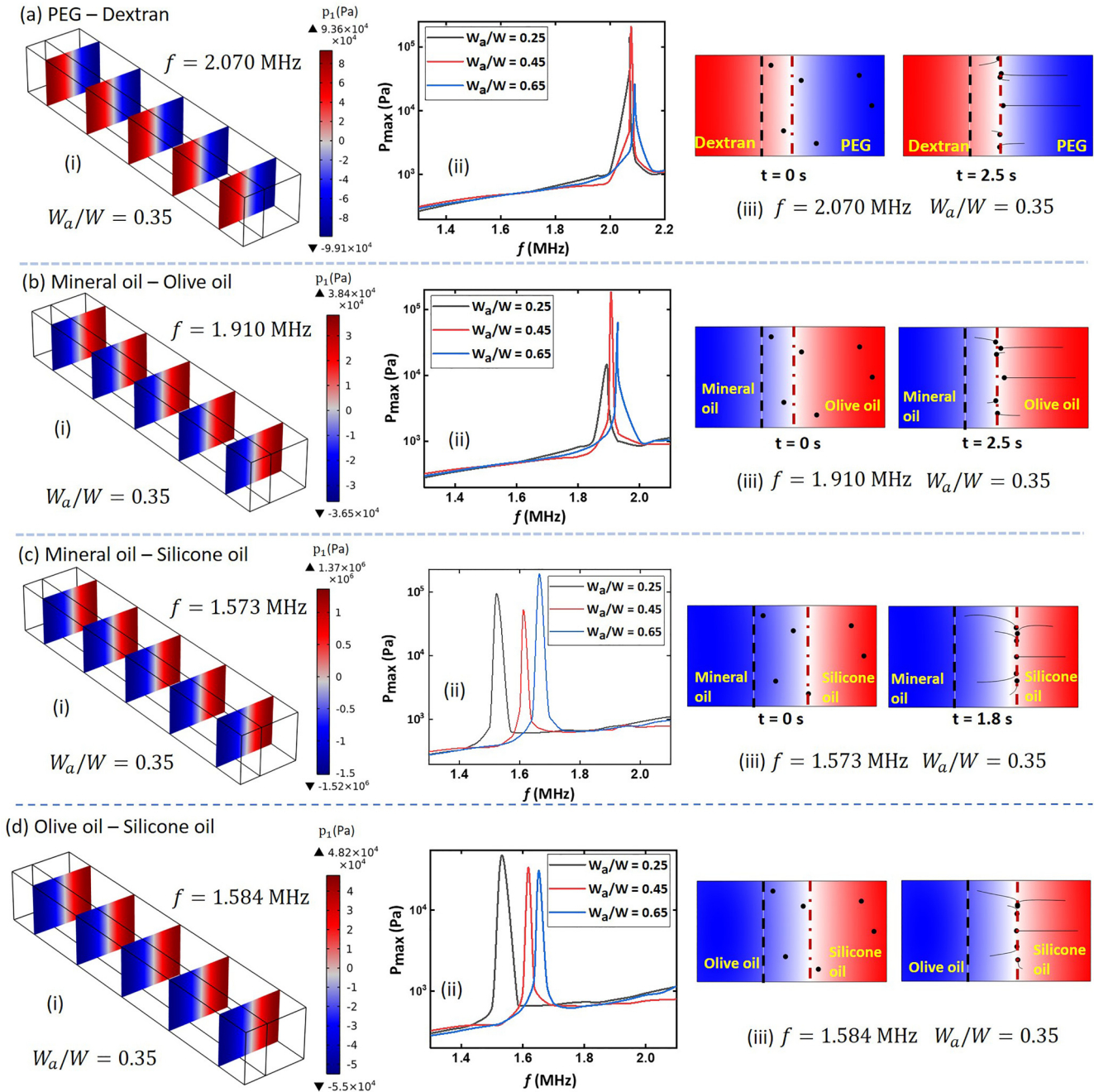


FIG. 2. Numerical simulation results for different coflow systems: (a) PEG-dextran with $(c_a/c_b) = 1$ and $(\rho_a/\rho_b) = 1$: (a-i) acoustic pressure contours, stream width ratio, $(W_a/W) = 0.35$, and actuation frequency, $f = 2.070$ MHz; (a-ii) variation of the maximum pressure amplitude (P_{max}) with actuation frequency (f), for $(W_a/W) = 0.25, 0.45$, and 0.65 ; (a-iii) particle trajectories showing particle focusing at the pressure N-P, $f = 2.070$ MHz, $(W_a/W) = 0.35$. (b) Mineral oil-olive oil with $(c_a/c_b) = 1$ and $(\rho_a/\rho_b) = 1$: (b-i) acoustic pressure contours, $(W_a/W) = 0.35$, and $f = 1.910$ MHz; (b-ii) variation of P_{max} with f , for $(W_a/W) = 0.25, 0.45$, and 0.65 ; (b-iii) particle trajectories showing particle focusing at the pressure N-P, $f = 1.910$ MHz, $(W_a/W) = 0.35$. (c) Mineral oil-silicone oil with $(c_a/c_b) \neq 1$ and $(\rho_a/\rho_b) \neq 1$: (c-i) total acoustic pressure field contours, $(W_a/W) = 0.35$, and, $f = 1.573$ MHz; (c-ii) variation of P_{max} with f for $(W_a/W) = 0.25, 0.45$, and 0.65 ; (c-iii) particle trajectories showing particle focusing at the pressure N-P, $f = 1.573$ MHz, $(W_a/W) = 0.35$. (d) Olive oil-silicone oil with $(c_a/c_b) \neq 1$ and $(\rho_a/\rho_b) \neq 1$: (d-i) total acoustic pressure field contours, $(W_a/W) = 0.35$, and, $f = 1.584$ MHz; (d-ii) variation of P_{max} with f for $(W_a/W) = 0.25, 0.45$, and 0.65 ; (d-iii) particle trajectories showing particle focusing at the pressure N-P, $f = 1.584$ MHz, $(W_a/W) = 0.35$.

We find that the speed of sound and density ratios individually affect the resonating frequency of coflow systems depending on the width ratio, irrespective of the characteristic impedance values. The variation of resonating frequency for

$(\rho_a/\rho_b) = 1$ and varying (c_a/c_b) , and for $(c_a/c_b) = 1$ and varying (ρ_a/ρ_b) , are presented in Appendix B. In coflow systems with $(c_a/c_b) \neq 1$ and $(\rho_a/\rho_b) \neq 1$, the component of the wave reflected from the interface is nonnegligible, and

therefore, the background pressure field can change significantly depending on the stream width ratio. We see that at half-wave resonance, the amplitude of the pressure field from simulations is of the order of 10^4 – 10^6 for all liquid combinations, which matches that predicted using the theoretical model [Eqs. (21)].

Further, we perform transient simulations with polystyrene particles of size $20\ \mu\text{m}$ using the particle-tracing module in COMSOL to demonstrate particle focusing at the pressure nodal plane at the resonant condition. The steady acoustic pressure profile at half wave resonance frequency obtained from the eigenfrequency analysis is coupled with the Particle Tracing Module, where the transient dynamics of polystyrene particles are analyzed. Further, we assumed a steady-state condition wherein the velocity of the liquids is neglected. The model for the particle dynamics considers primary acoustic radiation force due to the acoustic pressure and velocity fields at half-wave resonance and the drag force acting on the particles. The drag force acting on the particles is modeled using the linear Stokes drag formula given by $\mathbf{F}_D = 6\pi\mu r\mathbf{v}$, where \mathbf{v} is the particle velocity and r is the radius of the particle. The primary acoustic radiation force acting on the particles due to scattering of the acoustic wave from the particle surface is defined as $\mathbf{F}_p = -2\pi R^3 \nabla [f_1 \frac{1}{3\rho_0 c_0^2} p_{in}^2 - \frac{1}{2} f_2 \rho_0 v_{in}^2]$, where f_1 and f_2 are the monopole and dipole coefficients defined as $f_1 = 1 - [(\rho_0 c_0^2)/(\rho_p c_p^2)]$ and $f_2 = 2(\rho_p - \rho_0)/(2\rho_p + \rho_0)$ [41]. The above expression is derived by considering terms only up to monopole and dipole coefficients, and considering the Rayleigh limit and the shear waves inside the particle are neglected in calculating scattering coefficients from the particle. For simplicity, the interparticle radiation force due to multiscattering effects between the particles is neglected in the present study. The particles are randomly positioned in the liquid containing the pressure NP initially and get focused at the pressure NP when the system is exposed to BAWs, as shown in Fig. 3. For PEG-dextran and mineral oil-silicone oil systems, the particles move to the pressure NP in 2.5 s and 1.8 s, respectively. Next, we experimentally verify ultrasonic resonance conditions in the different coflow systems by observing the particle migration towards the pressure NP.

For different coflow systems, once the resonance frequency is obtained from the eigenfrequency analysis, the resonance mode is predicted from the theoretical model, and the first-order pressure profiles across the microchannel width are obtained using Eqs. (21), as shown in Fig. 3. The interface location is indicated by a black dotted line, with the pressure profiles in liquids a and b indicated by red and blue lines, respectively. Further, the location of the nodal plane is denoted by a brown color dotted line. The displacement amplitude of the oscillation is considered to be $l = 1\ \text{nm}$, and the oscillation frequency of the walls is taken from the frequency domain analysis as obtained from the simulations. For comparison with the simulation results, in the theoretical model, the interface location is taken to be at $W_a/W = 0.35$ for all the liquid combinations. In the case of PEG-dextran and mineral oil-olive oil coflow systems, the speeds of sound and the densities of liquids in a pair are approximately equal (see Table I), and therefore the pressure node is obtained at the center of the microchannel while actuating the system with resonating frequency $f_r = 2.070\ \text{MHz}$ and $f_r = 1.91\ \text{MHz}$,

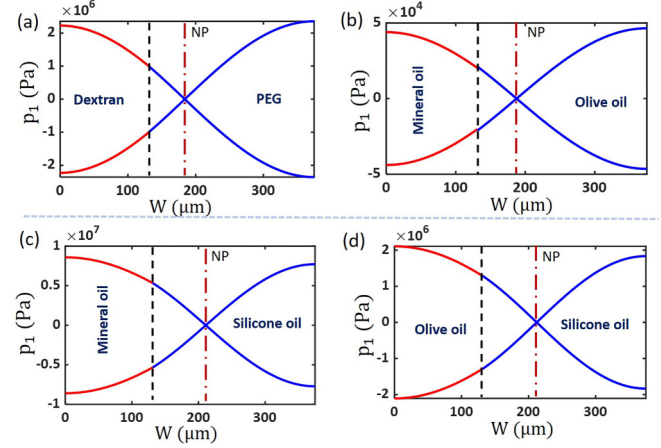


FIG. 3. The 1D first-order acoustic pressure fields plotted across the width of the microchannel for the different coflow combinations: (a) PEG and dextran, $W_a/W = 0.35$, $f_r = 2.07\ \text{MHz}$; (b) mineral oil and olive oil $W_a/W = 0.35$, $f_r = 1.91\ \text{MHz}$; (c) mineral oil and silicone oil, $W_a/W = 0.35$, $f_r = 1.573\ \text{MHz}$; (d) silicone oil and olive oil, $W_a/W = 0.35$, $f_r = 1.584\ \text{MHz}$. The interface location is indicated by a black dotted line with the pressure profiles in liquids a and b indicated by red and blue lines. The location of the nodal plane (NP) is denoted by a brown dotted line for each case.

respectively [see Figs. 3(a) and 3(b)]. The nodal plane (NP) is obtained exactly at the center of the microchannel for these pairs of liquids. For the mineral oil-silicone oil combination, since the speeds of sound and densities of the liquids in a pair are markedly different, when the liquids are actuated at the corresponding resonance frequency, $f_r = 1.573\ \text{MHz}$, half-wave resonance with NP away from the center of the microchannel is observed [see Fig. 3(c)]. Similarly, for the silicone oil-olive oil combination, the frequency of actuation to obtain the half-wave resonance is $f_r = 1.584\ \text{MHz}$, and the pressure amplitude variation across the channel width is shown in Fig. 3(d). We observed that the NP is formed away from the channel center towards the liquid having a higher speed of sound. Further, we also use the above model to predict the higher-order resonance modes in different coflow combinations (see Appendix C). We found that coflow systems with $(c_a/c_b) \approx 1$ and $(\rho_a/\rho_b) \approx 1$ can be actuated with a resonating frequency predicted from theory or simulations to obtain half-wave resonance, and the NP is formed exactly at the center of the microchannel. Coflow systems with $(c_a/c_b) \neq 1$ or $(\rho_a/\rho_b) \neq 1$ can also be actuated with a single resonating frequency obtained from the simulations to achieve the half-wave resonance where the NP has formed away from

TABLE II. Resonating frequency and acoustic contrast factor of polystyrene particles in different fluids.

Fluid	Resonating frequency (MHz)	Contrast factor
Mineral oil	1.97	0.608
Silicone oil	1.375	0.7094
Olive oil	1.93	0.5177
PEG	2.02	0.258
Dextran	2.018	0.1351

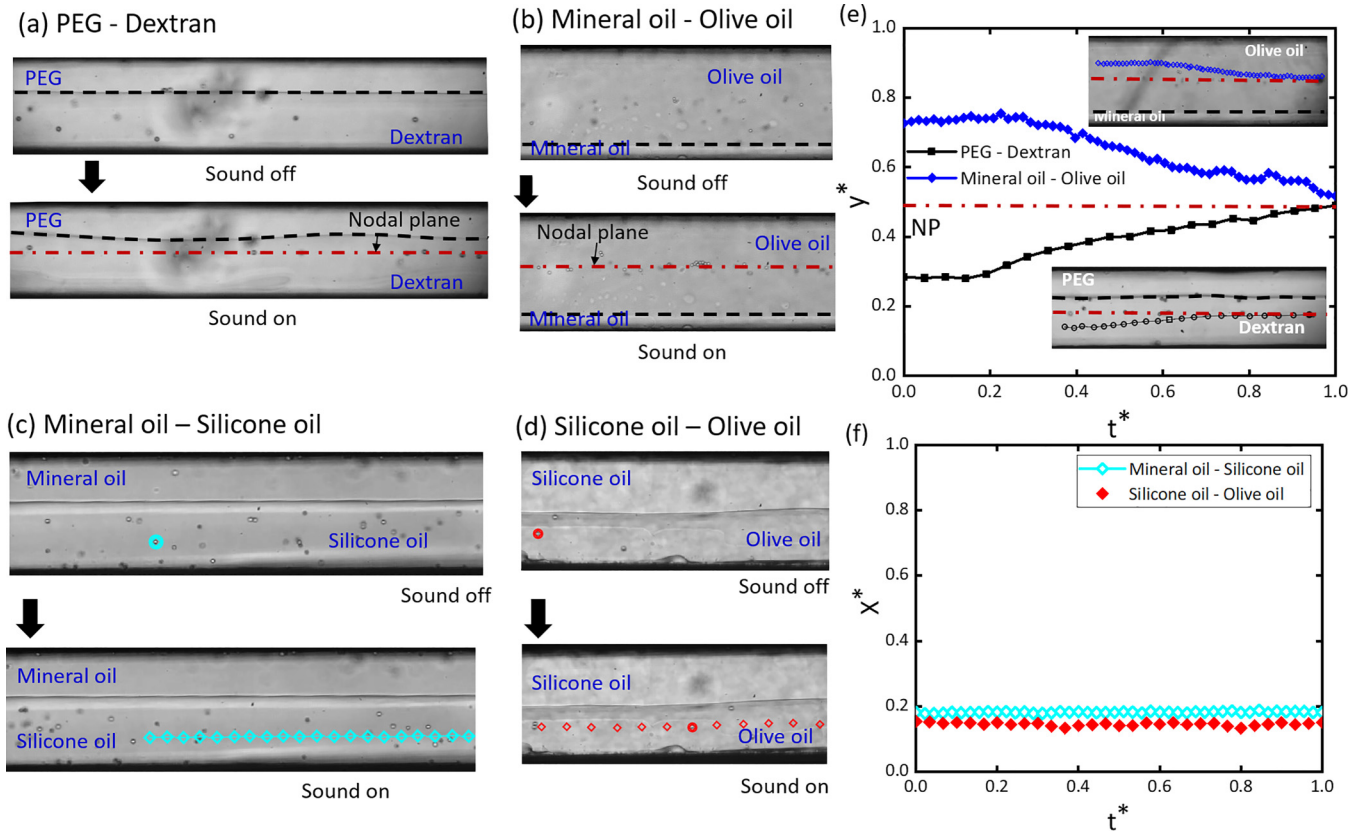


FIG. 4. The experimental images showing particle focusing or nonfocusing, suggesting the formation or absence of pressure NP, in different coflow systems with ultrasound OFF and ON: (a) PEG-dextran, $Q_{dex} = 15 \mu\text{l}/\text{min}$, $Q_{PEG} = 10 \mu\text{l}/\text{min}$, $f_r = 2.018 \text{ MHz}$; (b) mineral oil-olive oil, $Q_{mi} = 10 \mu\text{l}/\text{min}$, $Q_{ol} = 15 \mu\text{l}/\text{min}$, $f = 1.905 \text{ MHz}$; (c) mineral oil-silicone oil, $Q_{mi} = 15 \mu\text{l}/\text{min}$, $Q_{si} = 25 \mu\text{l}/\text{min}$, $W_1/W_2 = 0.72$, $f = 1.3\text{--}2.9 \text{ MHz}$; (d) silicone oil-olive oil, $Q_{si} = 5 \mu\text{l}/\text{min}$, $Q_{ol} = 10 \mu\text{l}/\text{min}$, $W_1/W_2 = 0.54$, $f = 1.3\text{--}2.9 \text{ MHz}$. Trajectories of particle migration towards the pressure NP with time in different coflow systems. (e) PEG-dextran and olive oil-mineral oil; insets show the experimental images of the particle motion towards NP. (f) Mineral oil-silicone oil and silicone oil-olive oil.

the channel center (see Fig. 3). For each coflow system with a fixed width of liquids, we can obtain a single resonating frequency from numerical simulations, and interestingly the single resonating frequency falls between the two resonating frequencies predicted using our theoretical model [Eq. (23)]. For example, in a mineral oil-silicone oil combination, with $W_a/W = 0.35$, the resonating frequency obtained from numerical simulations ($f_r = 1.573 \text{ MHz}$) is between the theoretically predicted resonant frequencies, $f_{mi} = 1.920 \text{ MHz}$ and $f_{si} = 1.375 \text{ MHz}$. So our model can predict a bound for the resonating frequency in the case where the speed of sound and density differ significantly.

Finally, we verify the resonance modes obtained from the eigenfrequency analysis and theoretical model using experiments. First, we performed experiments with a single liquid system to determine the half-wave resonating frequencies of individual liquids at which particles get focused at the pressure NP (see Appendix D). The resonating frequency and acoustic contrast factor of polystyrene particles in each of the liquids are presented in Table II. The density and speed of sound of polystyrene particle are given by $\rho_p = 1050 \text{ kg}/\text{m}^3$ and $c_p = 1700 \text{ m}/\text{s}$, respectively. The acoustic contrast factor is defined as $\psi = \frac{1}{3}f_1 + \frac{1}{2}f_2$. The experimental images of acoustic particle migration towards the pressure NP, and

the variation of nondimensional particle trajectory ($y^* = \frac{y}{W}$) with the normalized time ($t^* = \frac{t}{t_{\max}}$) in the different individual liquids, are shown in Appendix D. Here t_{\max} is the maximum time required for the particles to migrate to the pressure nodal plane. Next, we performed experiments with different coflow systems. In each case, particles are suspended in the liquid having a higher stream width covering the center of the channel where the pressure NP is expected at half-wave resonance condition. The system is then exposed to BAWs, and the actuating frequency is varied to achieve a half-wave resonance condition and particle migration toward the NP. The experimental images of particle focusing in the different immiscible coflow systems before and after the application of the BAWs are presented in Fig. 4. We have applied an acoustic power of 5.49 W to the coflowing system so that the acoustic energy density is low satisfying acoustocapillary number $Ca_{ac} < 1$ and thus preventing the relocation of liquids [5]. The acoustocapillary number, Ca_{ac} , is defined as the ratio of acoustic radiation force to the interfacial tension force that acts on the liquid-liquid interface. In each coflow system, the actuation frequency is varied in the range from 1.300 to 2.900 MHz to determine the resonating frequency at which particle focusing at the pressure NP is achieved. In PEG-dextran and mineral oil-olive oil systems, having comparable

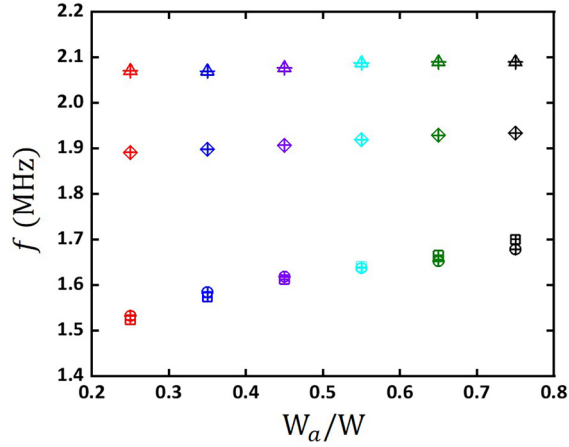


FIG. 5. Variation of resonance frequency with the stream width ratio for different immiscible coflow systems: mineral oil-silicone oil (■), olive oil-silicone oil (●), PEG-dextran (▲), and olive oil-mineral oil (◆).

speed of sound values (see Table I), we find that the particles are focused at the center of the microchannel suggesting the formation of a pressure NP at the channel center. The variation of nondimensional particle trajectory (y^*) with the normalized time (t^*) is presented in Fig. 4. The resonating frequency at which particle focusing is observed is found to be 2.018 MHz and 1.905 MHz, respectively, for PEG-dextran and mineral oil-olive oil combinations, which is in agreement with the predictions of both the analytical model and numerical simulations. In this case, with $(c_a/c_b) = 1$, and $(\rho_a/\rho_b) = 1$, the resonant frequency is found to be independent of the stream width ratios. In the case of mineral oil-silicone oil and silicone oil-olive oil combinations, owing to a marked difference in the speeds of sound in the liquids, the resonating frequency is sensitive to the variation of stream width ratio as discussed earlier [see Fig. 3(c) and 3(d)]. In this case, with $(c_a/c_b) \neq 1$, and $(\rho_a/\rho_b) \neq 1$, experimentally finding the exact resonating frequency is extremely challenging since the resonance frequency for a given coflow system is dependent on the stream width ratio and sensitive to the frequency variation in the kHz range. In such systems, the acoustic resonance conditions could be easily predicted using the 3D numerical model.

The variation of resonance frequency with the stream width ratio for the different coflow systems is presented in Fig. 5. We find that for PEG-dextran and olive oil-mineral oil systems with $(c_a/c_b) = 1$ and $(\rho_a/\rho_b) = 1$, the resonating frequency is independent of the width ratio, (W_a/W). For coflow systems with $(c_a/c_b) \neq 1$ or $(\rho_a/\rho_b) \neq 1$, the resonating frequency varies with the stream width ratio. In our study, the liquid streams are arranged in such a way that the resonating frequency corresponding to fluid a is higher than that of fluid b , and therefore, by increasing the width of the stream a (i.e., W_a), the resonating frequency increases. As discussed, irrespective of the stream width ratio, the resonating frequency for a given coflow system falls within the two resonating frequency values corresponding to the two individual single-fluid systems. Further, by varying the frequency of actuation and stream width ratio, we show that a maximum pressure amplitude higher than 10^4 Pa is achieved at the resonance

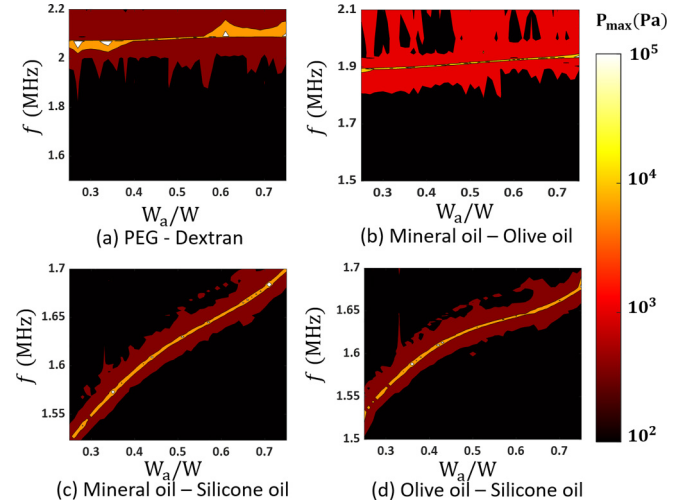


FIG. 6. Maximum acoustic pressure amplitude contours as a function of actuating frequency and width ratio of liquids in a coflow system: (a) PEG-dextran, (b) mineral oil-olive oil, (c) mineral oil-silicone oil, and (d) olive oil-silicone oil. The maximum pressure amplitude is more significant than 10^4 Pa at the resonance condition, irrespective of the coflow systems and width ratios.

condition for a coflowing system when actuating with the incoming pressure amplitude of 10^6 Pa. The contour plot of maximum acoustic pressure amplitude (P_{\max}) as a function of stream width ratio and actuating frequency for the different pair of liquids is presented in Fig. 6. For the dextran-PEG and mineral oil-olive oil combination, the P_{\max} is higher than 10^4 Pa along the line where the actuation frequency remains constant [see Figs. 6(a) and 6(b)]. Thus, the resonating frequency for a coflow system with comparable fluid parameters is independent of the width ratio. However, for the cases where the fluid parameters are significantly different such as mineral oil-silicone oil and olive oil-silicone oil, we observed that the P_{\max} is higher than 10^4 Pa for a particular actuation frequency and a given stream width. These results suggest that the resonating frequency for the fluid pair with different speed of sound and density is highly sensitive to the stream width of the two liquids. The results obtained from the eigenfrequency analysis are in good agreement with the predictions of the 1D analytical model for a displacement amplitude of oscillation of 1 nm [Eq. (21)]. To summarize, a 3D plot of maximum pressure amplitude as a function of actuation frequency and stream width ratio is presented in Fig. 13 (see Appendix E).

VI. CONCLUSION

In summary, we studied ultrasonic resonance in a coflow system with a pair of immiscible liquids in a microchannel exposed to BAWs. We discovered that resonance could be achieved in a coflow system by actuating at a single resonating frequency whose value is governed by the ratio of the speeds of sound, densities, and the widths of the liquids. The resonating frequency of a system with liquids of equal speeds of sound and densities is independent of the width ratio. On the other hand, the resonating frequency of a coflow system with unequal speeds of sound and densities

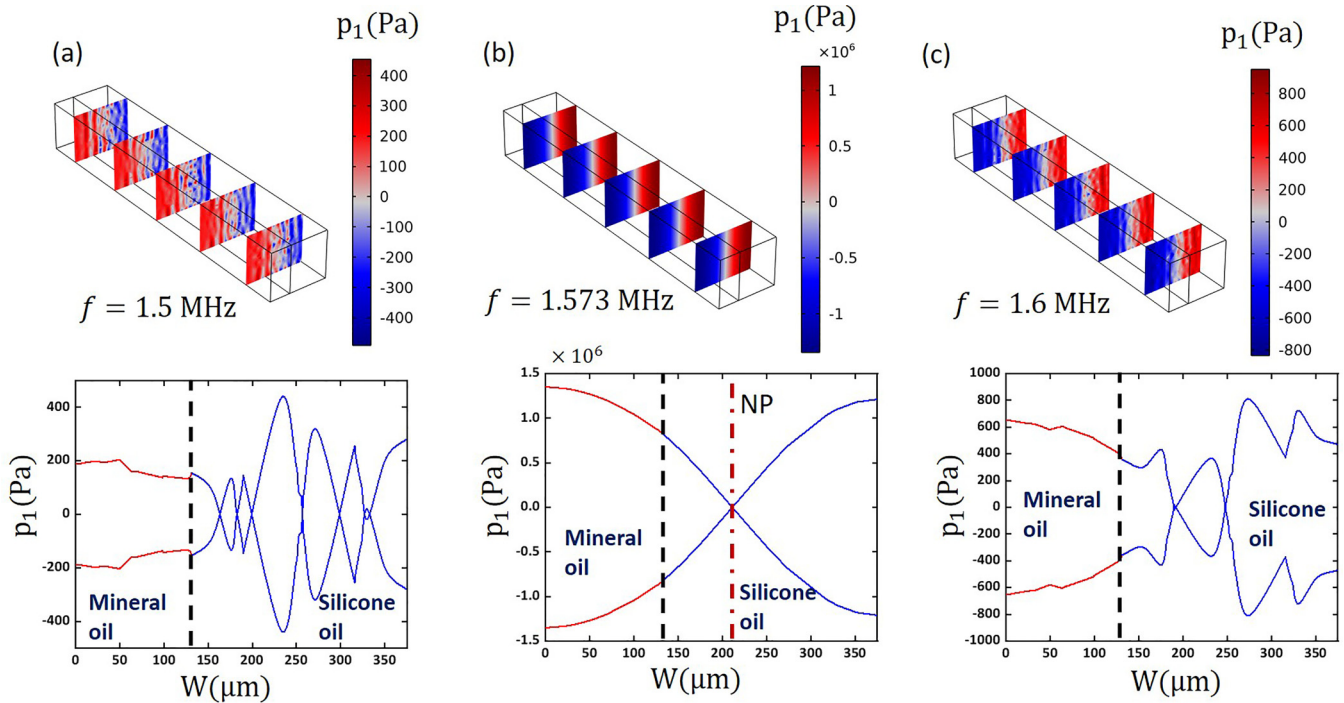


FIG. 7. Variation of acoustic pressure field (p_1) for the mineral oil-silicone oil case for the stream width ratio, $\frac{W_a}{W} = 0.35$. The pressure field contours across the domain and the pressure field variation across the width of the microchannel are shown for the actuation frequency (a) $f = 1.5$ MHz, (b) $f = 1.573$ MHz, and (c) $f = 1.6$ MHz. This shows that the half-wave resonance is obtained at the frequency $f = f_r = 1.573$ MHz, the resonating frequency of the coflowing system for the given width ratio, $\frac{W_a}{W} = 0.35$. The half wave pressure node is not formed when the system is actuated at frequency, $f = 1.5$ MHz and $f = 1.6$ MHz.

is proportional to the stream width ratio. In the latter scenario, a frequency sweep can be used to identify the resonating frequency from numerical simulations, which is found to be between the resonant frequencies corresponding to the individual liquids. The resonating frequency predicted using eigenfrequency analysis from simulations is used in the theoretical model to predict the acoustic pressure field variation along the width of the channel. We found that a pressure nodal plane is formed inside the channel when the system is actuated with the predicted resonating frequency from simulations, irrespective of the density and speed of sound ratios of the two fluids. Both from the theoretical model and simulations, we predicted a maximum pressure amplitude greater than 10^4 Pa at resonance condition considering the lossless and inviscid medium. Experiments were used to validate the analytical model and numerical simulations, which showed an excellent match in terms of the resonating frequency for liquids with equal density and speed of sound. In the case of liquids with marked density and speed of sound contrast, the resonating frequency varies in the kHz range with the variation in stream width ratio. Therefore, it is extremely difficult to identify the resonating frequency precisely to experimentally observe particle migration towards the nodal plane. However, a half-wave resonance mode can be predicted using eigenfrequency analysis for a fluid pair irrespective of density and speed of sound ratios. At the half-wave resonance condition, in a coflow system with equal speeds of sound and density, the pressure nodal plane is formed at the channel center, while in a coflow system with unequal speeds of sound and density, the pressure nodal plane is shifted

away from the channel center toward the liquid having a higher speed of sound. The present study reveals resonance conditions in an immiscible coflow system that may find relevance in biochemical applications involving bulk acoustic waves.

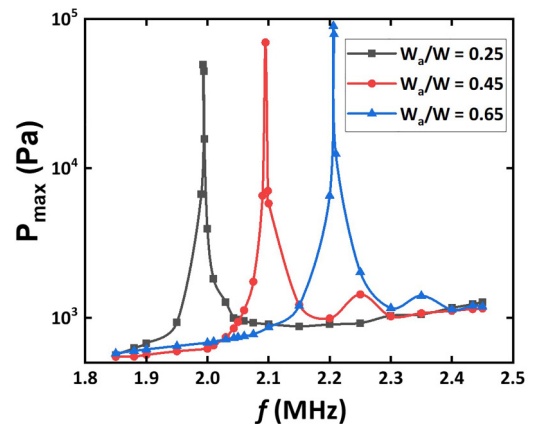


FIG. 8. Variation of maximum pressure amplitude (P_{\max}) with the actuation frequency (f) for a coflowing fluids with impedance match, i.e., $Z_a = Z_b = 2.045 \times 10^6$ kg/m² s. The density of fluid a and fluid b are $\rho_a = 1120$ kg/m³ and $\rho_b = 1410$ kg/m³ (i.e., $\rho_a \neq \rho_b$). The speed of sound in fluid a and fluid b is $C_a = 1825.45$ kg/m³ and $C_b = 1410$ kg/m³ (i.e., $C_a \neq C_b$). The resonating frequency for the coflowing fluids with $W_a/W=0.25$, 0.45 , and 0.65 is given by 1.993 , 2.095 , and 2.206 MHz respectively. The resonating frequencies lie between the theoretically obtained frequency for the fluid a and fluid b (i.e., $f_a = 2.434$ MHz $>$ f_r $>$ $f_b = 1.88$ MHz).

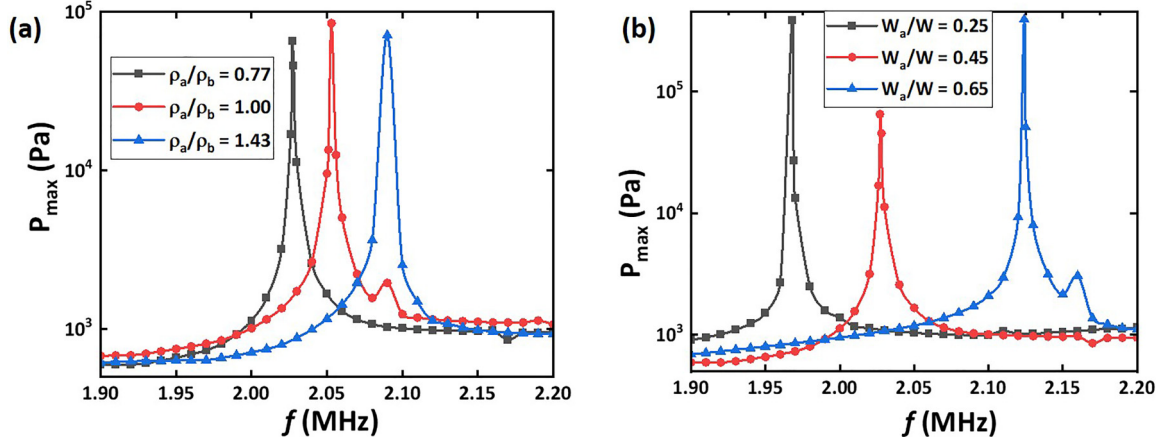


FIG. 9. (a) Variation of maximum pressure amplitude (P_{\max}) with the actuation frequency (f) for coflowing fluids as a function of density variations with $(c_a/c_b) = 1$ and $(W_a/W) = 0.45$. The resonating frequency for $(\rho_a/\rho_b) = 0.77, 1.00,$ and 1.43 is given by $f_r = 2.027, 2.053,$ and 2.090 MHz, respectively. (b) Variation of the maximum pressure amplitude (P_{\max}) with actuation frequency (f), for $(W_a/W) = 0.25, 0.45,$ and 0.65 with $(c_a/c_b) = 1$ and $(\rho_a/\rho_b) = 0.77$. The resonating frequency for width ratios $(W_a/W) = 0.25, 0.45,$ and 0.65 is given by $f_r = 1.968, 2.027,$ and 2.124 MHz, respectively.

ACKNOWLEDGMENTS

A.K.S. thanks the Department of Science & Technology (DST), Government of India for providing financial support in the form of the Swarnajayanti Fellowship Award via Grant No. DST/SJF/ETA-03/2017-18. The support from the Indian Institute of Technology Madras to the Micro Nano Bio-Fluidics Group under the funding for Institutions of Eminence scheme of Ministry of Education, Government of India [Sanction No. 11/9/2019-U.3(A)] is also acknowledged.

APPENDIX A: ACOUSTIC PRESSURE FIELD VARIATION AS A FUNCTION OF ACTUATION FREQUENCY

The acoustic pressure field contours for the mineral oil-silicone oil as cofluids actuated at different frequencies are shown in Fig. 7. The pressure variation along the width of the channel is also plotted at the midplane. It can be seen that the half-wave pressure nodal plane is obtained at the frequency $f = 1.573$ MHz. However, the half-wave pressure node formation is not observed when the system is actuated at frequencies, $f = 1.5$ MHz and 1.6 MHz.

APPENDIX B: EFFECTS OF DENSITY AND IMPEDANCE CONTRAST ON THE RESONATING FREQUENCY

Figure 8 shows the variation of maximum pressure amplitude as a function of the actuation frequency for two fluids with equal impedances. The resonating frequencies vary as a function of the interface irrespective of no impedance contrast between the fluids. This shows that the resonating frequency for a coflow system depends on the individual values of the density and speed of sound in the two fluids.

For a fluid pair with an equal speed of sound, the pressure field variation as a function of actuation frequency and density contrast is shown in Fig. 9. We observed that for a fixed width ratio (i.e., $\frac{W_a}{W} = 0.45$), the resonating frequency doesn't vary significantly with the density contrast between the fluids [see Fig. 9(a)]. The resonating frequency for $(\rho_a/\rho_b) = 0.77, 1.00,$ and 1.43 is given by $f_r = 2.027, 2.053,$ and 2.090 MHz, respectively. However, a significant difference in the resonating frequency can be observed when the width of the two streams is varied. The resonating frequency for width ratios $(W_a/W) = 0.25, 0.45,$ and 0.65 is given by $f_r = 1.968, 2.027,$ and 2.124 MHz, respectively. The results

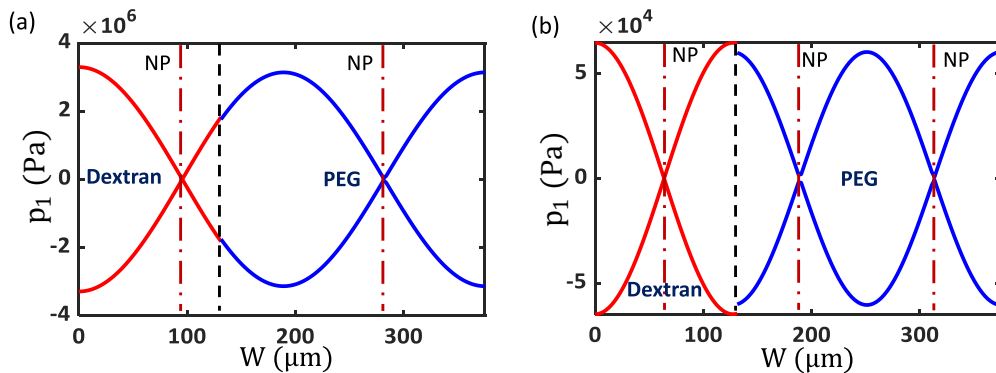


FIG. 10. The 1D first-order pressure field plotted against the width of the microchannel for the coflowing fluids PEG and dextran. (a) Second-order modes $m = n = 2$, two nodal planes are observed; and (b) third-order modes $m = n = 3$, three nodal planes can be seen irrespective of the location of the fluid-fluid interface.

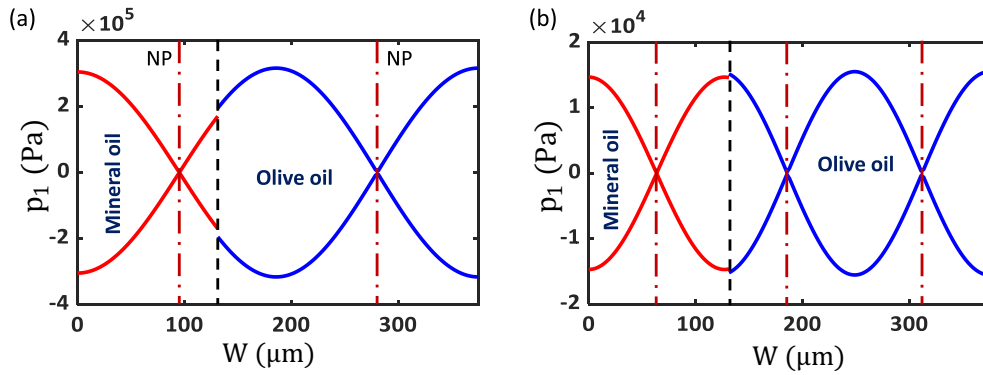


FIG. 11. The 1D first-order pressure field plotted against the width of the microchannel for the coflowing fluids mineral oil and olive oil. (a) Second-order modes $m = n = 2$, two nodal planes are observed; and (b) third-order modes $m = n = 3$, three nodal planes can be seen irrespective of the location of the fluid-fluid interface.

imply that even with the equal speed of sound in the two fluids, there is an influence of the density contrast on the resonating frequency of the system.

APPENDIX C: HIGHER-ORDER RESONANCE MODES

We study higher-order acoustic modes for the coflowing fluids inside the rectangular microchannel for the cases where the speed of sound in the fluids a and b is equal (i.e., $c_a \approx c_b$). Second-order resonance modes (i.e., $m = n = 2$) are obtained for the PEG-dextran combination, and the amplitude of the first-order pressure field is plotted as shown

in Fig. 10. We observed two pressure node formations (one in each fluid) for second-order modes, i.e., $m = n = 2$ [see Fig. 10(a)]. Similarly, third harmonic modes can be obtained for the mode number $m = n = 3$. In this case, a pressure nodal plane is formed in PEG, and the other two pressure nodes are observed in the dextran phase, as depicted in Fig. 10(b). The corresponding resonating frequencies to obtain the second- and third-order modes are given by $f_r = 4.14$ MHz and $f_r = 6.21$ MHz respectively. Interestingly, an immiscible fluid-fluid interface doesn't affect the formation of the pressure nodal planes when actuated at the resonance frequency.

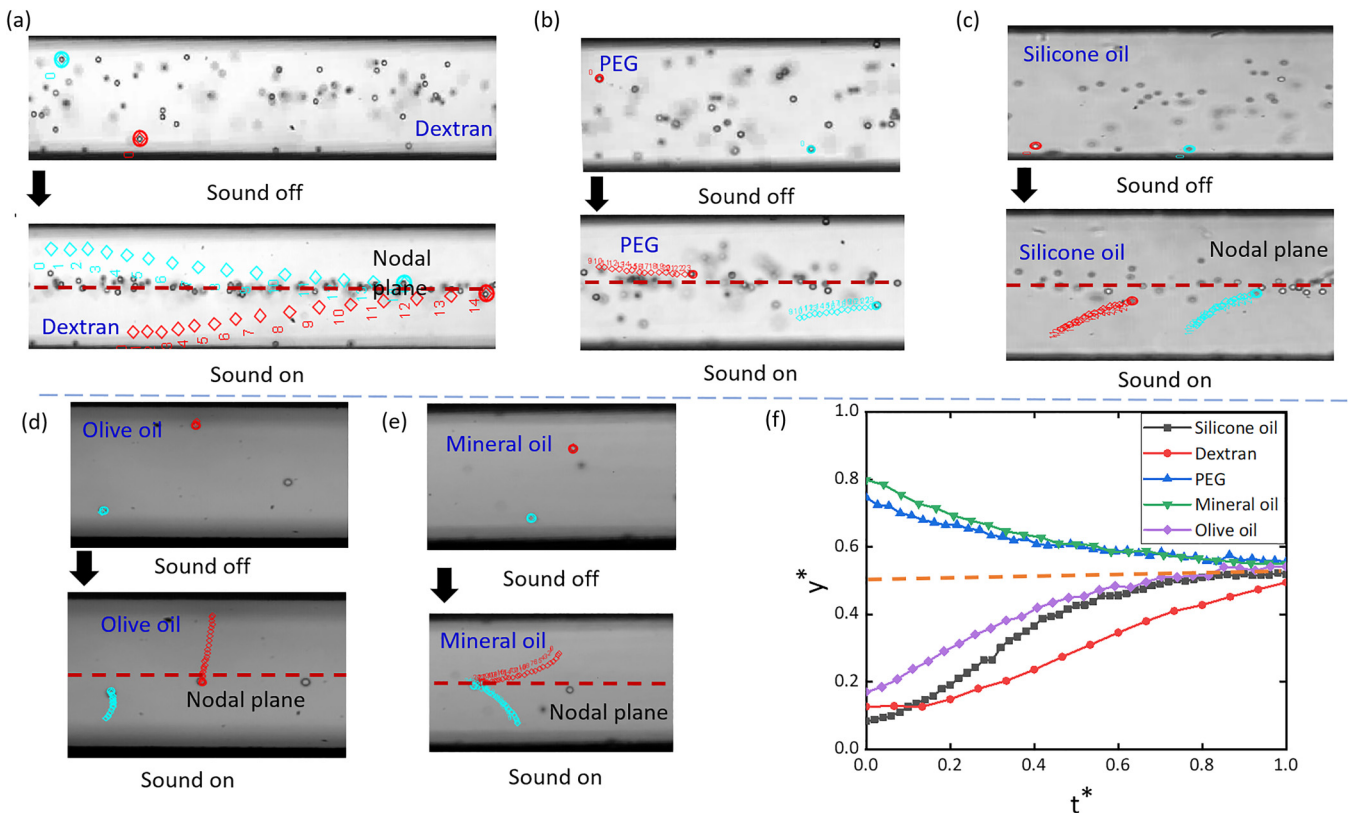


FIG. 12. Experimental images of particle focusing towards the center of the microchannel in a single-fluid case: (a) dextran (10% wt), $f = 2.018$ MHz, (b) PEG (5% wt), $f = 2.02$ MHz, (c) silicone oil, $f = 1.375$ MHz, (d) olive oil, $f = 1.93$ MHz, (e) mineral oil, $f = 1.97$ MHz, (f) variation of the trajectory of polystyrene particles with time in different fluids.

Similarly, for the mineral oil and olive oil as the fluid combination, we obtained the higher-order acoustic modes for mode numbers 2 and 3, respectively. The results are presented in terms of acoustic pressure amplitudes in Fig. 11. The corresponding actuation frequencies for the second- and third-order modes are given by $f_r = 3.78$ MHz and $f_r = 5.67$ MHz, respectively. Two pressure nodes are observed for second-order modes for $m = n = 2$, while the three nodal planes are obtained for the mode number, $m = n = 3$. The location of the interface doesn't have any impact on the formation of the acoustic modes when actuated with the resonating frequencies for the fluid combinations.

APPENDIX D: PRESSURE NODAL PLANE IN A SINGLE FLUID

In the present case, the actuation frequency of the transducer considered is 2 MHz. The half-width of the microchannel is kept at $375 \mu\text{m}$ such that the pressure node is formed at the center of the microchannel for the fluid with a speed of sound around 1500 m/s . Polystyrene particles of sizes $15\text{--}20 \mu\text{m}$ are suspended in each liquid and actuated with an acoustic wave to obtain the resonating frequency of the corresponding fluids. The density and the speed of the sound of the particle are 1050 kg/m^3 and 1700 m/s . The contrast factor of the particle in different fluids is calculated and presented in Table II. The contrast factor is of the same order in all the liquids. Therefore, the acoustic contrast factor is nonnegligible in all fluids.

Further, we have observed for a single fluid that the particles are getting focused in all fluids. The particle trajectories towards the pressure nodal plane considering a single fluid are shown in Fig. 12. We observed that depending on the speed of sound in each fluid, the resonating frequency of the system varies since the width of the microchannel is kept constant. Although the actuation frequency of the transducer used is 2 MHz, we obtained the resonating frequency for the different fluids in the range $1.3\text{--}2$ MHz (see Table II). The variation of nondimensional particle trajectory ($y^* = y/W_2$) with the normalized time ($t^* = t/t_{\text{max}}$) towards the center of the microchannel in each fluid is presented in Fig. 12(f). Here t_{max} is the time the particle takes to traverse to the center of the microchannel.

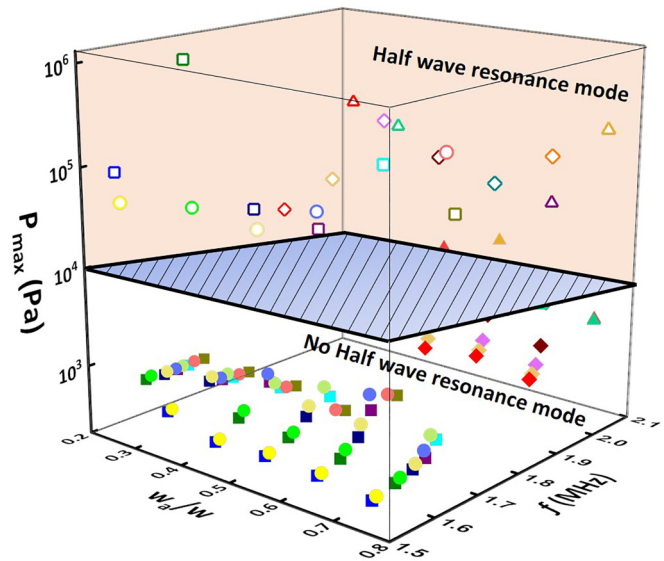


FIG. 13. Formation and absence of half wave resonance mode in various immiscible coflow systems represented in terms of the maximum pressure amplitude depending upon the stream width ratios and actuation frequency. The maximum pressure amplitude is more significant than 10^4 at the resonance condition, irrespective of the coflow systems and width ratios: mineral oil-silicone oil (■), olive oil-silicone oil (●), PEG-dextran (▲), and olive oil-mineral oil (◆).

APPENDIX E: MAXIMUM PRESSURE AMPLITUDE AS A FUNCTION OF ACTUATION FREQUENCY AND WIDTH RATIO

We found that the resonating frequency of the system varies when the width of the two fluid streams changes inside the microchannel. Also, the acoustic pressure amplitude is found to be maximum at the resonating frequency from the eigenfrequency analysis. The results are summarized in a 3D plot where the pressure amplitude is plotted as a function of actuation frequency and stream width ratio as shown in Fig. 13. By doing a frequency sweep for a given width ratio the resonating frequency of the coflowing fluids is obtained.

- [1] J. J. Hawkes, R. W. Barber, D. R. Emerson, and W. T. Coakley, Continuous cell washing and mixing driven by an ultrasound standing wave within a microfluidic channel, *Lab Chip* **4**, 446 (2004).
- [2] S. Karthick, P. N. Pradeep, P. Kanchana, and A. K. Sen, Acoustic impedance-based size-independent isolation of circulating tumour cells from blood using acoustophoresis, *Lab Chip* **18**, 3802 (2018).
- [3] P. Augustsson, L. B. Åberg, A. M. K. Swärd-Nilsson, and T. Laurell, Buffer medium exchange in continuous cell and particle streams using ultrasonic standing wave focusing, *Microchim. Acta* **164**, 269 (2009).

- [4] A. Lenshof, C. Magnusson, and T. Laurell, Acoustofluidics 8: Applications of acoustophoresis in continuous flow microsystems, *Lab Chip* **12**, 1210 (2012).
- [5] E. Hemachandran, S. Z. Hoque, T. Laurell, and A. K. Sen, Reversible Stream Drop Transition in a Microfluidic Coflow System via On Demand Exposure to Acoustic Standing Waves, *Phys. Rev. Lett.* **127**, 134501 (2021).
- [6] J. Friend and L. Y. Yeo, Microscale acoustofluidics: Microfluidics driven via acoustics and ultrasonics, *Rev. Mod. Phys.* **83**, 647 (2011).
- [7] W. Connacher, N. Zhang, A. Huang, J. Mei, S. Zhang, T. Gopesh, and J. Friend, Micro/nano acoustofluidics: Materials,

- phenomena, design, devices, and applications, *Lab Chip* **18**, 1952 (2018).
- [8] Y. Chen, M. Wu, L. Ren, J. Liu, P. H. Whitley, L. Wang, and T. J. Huang, High-throughput acoustic separation of platelets from whole blood, *Lab Chip* **16**, 3466 (2016).
- [9] I. Leibacher, P. Reichert, and J. Dual, Microfluidic droplet handling by bulk acoustic wave (BAW) acoustophoresis, *Lab Chip* **15**, 2896 (2015).
- [10] B. Hammarström, T. Laurell, and J. Nilsson, Seed particle-enabled acoustic trapping of bacteria and nanoparticles in continuous flow systems, *Lab Chip* **12**, 4296 (2012).
- [11] P. Li and T. J. Huang, Applications of acoustofluidics in bioanalytical chemistry, *Anal. Chem.* **91**, 757 (2019).
- [12] P. Ohlsson, M. Evander, K. Petersson, L. Mellhammar, A. Lehmusvuori, U. Karhunen, M. Soikkeli, T. Seppä, E. Tuunainen, A. Spangar *et al.*, Integrated acoustic separation, enrichment, and microchip polymerase chain reaction detection of bacteria from blood for rapid sepsis diagnostics, *Anal. Chem.* **88**, 9403 (2016).
- [13] J. T. Karlsen and H. Bruus, Acoustic Tweezing and Patterning of Concentration Fields in Microfluidics, *Phys. Rev. Appl.* **7**, 034017 (2017).
- [14] W. Qiu, J. T. Karlsen, H. Bruus, and P. Augustsson, Experimental Characterization of Acoustic Streaming in Gradients of Density and Compressibility, *Phys. Rev. Appl.* **11**, 024018 (2019).
- [15] G. P. Gautam, R. Gurung, F. A. Fencl, and M. E. Piyasena, Separation of sub-micron particles from micron particles using acoustic fluid relocation combined with acoustophoresis, *Anal. Bioanal. Chem.* **410**, 6561 (2018).
- [16] L. Angelica and C. Mauricio, Determination of the secondary Bjerknes force in acoustic resonators on ground and in microgravity conditions, *Microgr. Sci. Technol.* **28**, 11 (2016).
- [17] G. T. Silva and H. Bruus, Acoustic interaction forces between small particles in an ideal fluid, *Phys. Rev. E* **90**, 063007 (2014).
- [18] S. Z. Hoque and A. K. Sen, Interparticle acoustic radiation force between a pair of spherical particles in a liquid exposed to a standing bulk acoustic wave, *Phys. Fluids* **32**, 072004 (2020).
- [19] S. Z. Hoque, A. Nath, and A. K. Sen, Dynamical motion of a pair of microparticles at the acoustic pressure nodal plane under the combined effect of axial primary radiation and interparticle forces, *J. Acoust. Soc. Am.* **150**, 307 (2021).
- [20] T. Laurell, F. Petersson, and A. Nilsson, Chip integrated strategies for acoustic separation and manipulation of cells and particles, *Chem. Soc. Rev.* **36**, 492 (2007).
- [21] H. Bruus, Acoustofluidics 2: Perturbation theory and ultrasound resonance modes, *Lab Chip* **12**, 20 (2012).
- [22] A. Nath and A. K. Sen, Acoustic Behavior of a Dense Suspension in an Inhomogeneous Flow in a Microchannel, *Phys. Rev. Appl.* **12**, 054009 (2019).
- [23] A. Nath, L. Malik, and A. K. Sen, Combined acoustic relocation and acoustophoretic migration for particle transfer between co-flowing fluids in a microchannel, *Phys. Rev. Fluids* **6**, 044201 (2021).
- [24] L. Johansson, S. Johansson, F. Nikolajeff, and S. Thorslund, Effective mixing of laminar flows at a density interface by an integrated ultrasonic transducer, *Lab Chip* **9**, 297 (2009).
- [25] P. Augustsson, J. T. Karlsen, H. W. Su, H. Bruus, and J. Voldman, Iso-acoustic focusing of cells for size-insensitive acousto-mechanical phenotyping, *Nat. Commun.* **7**, 1155 (2016).
- [26] J. T. Karlsen, P. Augustsson, and H. Bruus, Acoustic Force Density Acting on Inhomogeneous Fluids in Acoustic Fields, *Phys. Rev. Lett.* **117**, 114504 (2016).
- [27] J. T. Karlsen, W. Qiu, P. Augustsson, and H. Bruus, Acoustic Streaming and Its Suppression in Inhomogeneous Fluids, *Phys. Rev. Lett.* **120**, 054501 (2018).
- [28] L. D. Landau and E. M. Lifshitz, Fluid mechanics, in *Landau and Lifshitz: Course of Theoretical Physics*, 2nd ed. (Image, Rochester, NY, 1987), Vol. 6.
- [29] C. Cinbis and N. N. Mansour, Effect of surface tension on the acoustic radiation pressure-induced motion of the water-air interface, *J. Acoust. Soc. Am.* **94**, 2365 (1993).
- [30] M. J. Marr-Lyon, D. B. Thiessen, and P. L. Marston, Passive Stabilization of Capillary Bridges in Air with Acoustic Radiation Pressure, *Phys. Rev. Lett.* **86**, 2293 (2001).
- [31] B. Isenmann, A. Nicolas, R. Wunenburger, S. Manneville, and J. P. Delville, Deformation of acoustically transparent fluid interfaces by the acoustic radiation pressure, *Europhys. Lett.* **83**, 34002 (2008).
- [32] B. Isenmann, R. Wunenburger, H. Chraïbi, M. Gandil, and J. P. Delville, Unsteady deformations of a free liquid surface caused by radiation pressure, *J. Fluid Mech.* **682**, 460 (2011).
- [33] G. Kim, S. Cheng, L. Hong, J. T. Kim, K. C. Li, and L. P. Chamorro, On the acoustic fountain types and flow induced with focused ultrasound, *J. Fluid Mech.* **909**, 227 (2020).
- [34] R. Lirette, J. Mobley, and L. Zhang, Ultrasonic Extraction and Manipulation of Droplets from a Liquid-Liquid Interface with Near-Field Acoustic Tweezers, *Phys. Rev. Appl.* **12**, 061001 (2019).
- [35] E. Hemachandran, S. Karthick, T. Laurell, and A. K. Sen, Relocation of coflowing immiscible liquids under acoustic field in a microchannel, *Europhys. Lett.* **125**, 54002 (2019).
- [36] E. Hemachandran, T. Laurell, and A. K. Sen, Continuous Droplet Coalescence in a Microchannel Coflow Using Bulk Acoustic Waves, *Phys. Rev. Appl.* **12**, 044008 (2019).
- [37] P. B. Muller and H. Bruus, Theoretical study of time-dependent, ultrasound induced acoustic streaming in microchannels radiation, *Phys. Rev. E* **92**, 063018 (2015).
- [38] P. Glynn-Jones, R. J. Boltryk, and M. Hill, Acoustofluidics 9: Modelling and applications of planar resonant devices for acoustic particle manipulation, *Lab Chip* **12**, 1417 (2012).
- [39] T. Baasch and J. Dual, Acoustic Radiation Force on a Spherical Fluid or Solid Elastic Particle Placed Close to a Fluid or Solid Elastic Half-Space, *Phys. Rev. Appl.* **14**, 024052 (2020).
- [40] S. Hazra, A. Nath, S. K. Mitra, and A. K. Sen, Dynamics of rigid particles in a confined flow of viscoelastic and strongly shear-thinning fluid at very small Reynolds number, *Phys. Fluids* **33**, 052001 (2021).
- [41] H. Bruus, Acoustofluidics 7: The acoustic radiation force on small particles, *Lab Chip* **12**, 1014 (2012).